Biochimica et Biophysica Acta 1817 (2012) 811–818

Contents lists available at SciVerse ScienceDirect

Biochimica et Biophysica Acta

journal homepage: www.elsevier.com/locate/bbabio

Tyrosine triad at the interface between the Rieske iron–sulfur protein, cytochrome c_1 and cytochrome c_2 in the bc_1 complex of *Rhodobacter capsulatus*

John A. Kyndt *, John C. Fitch, Robert E. Berry, Matt C. Stewart, Kevin Whitley, Terry E. Meyer, F. Ann Walker, Michael A. Cusanovich [1]

Department of Chemistry and Biochemistry, University of Arizona, Tucson, AZ, 85721, USA

ARTICLE INFO

Article history:
Received 26 July 2011
Received in revised form 20 January 2012
Accepted 20 January 2012
Available online 28 January 2012

Keywords:
Rhodobacter capsulatus
BC1 complex
Mutagenesis
Redox potential

ABSTRACT

A triad of tyrosine residues (Y152–154) in the cytochrome c_1 subunit (C1) of the *Rhodobacter capsulatus* cytochrome bc_1 complex (BC1) is ideally positioned to interact with cytochrome c_2 (C2). Mutational analysis of these three tyrosines showed that, of the three, Y154 is the most important, since its mutation to alanine resulted in significantly reduced levels, destabilization, and inactivation of BC1. A second-site revertant of this mutant that regained photosynthetic capacity was found to have acquired two further mutations—A181T and A200V. The Y152Q mutation did not change the spectral or electrochemical properties of C1, and showed wild-type enzymatic C2 reduction rates, indicating that this mutation did not introduce major structural changes in C1 nor affect overall activity. Mutations Y153Q and Y153A, on the other hand, clearly affect the redox properties of C1 (e.g. by lowering the midpoint potential as much as 117 mV in Y153Q) and the activity by 90% and 50%, respectively. A more conservative Y153F mutant on the other hand, behaves similarly to wild-type. This underscores the importance of an aromatic residue at position Y153, presumably to maintain close packing with P184, which modeling indicates is likely to stabilize the sixth heme ligand conformation.

1. Introduction

Electron transfer processes are of indisputable importance in metabolic pathways in most living organisms. They are essential for photosynthesis and respiration, in which energy gained from capturing light or oxidation of nutrients is used to generate ATP. Cytochrome bc_1 (BC1; also called the bc_1 complex or ubiquinol-cytochrome *c* reductase) and the analogous cytochrome b_6f complex, are ubiquitous membrane proteins found in mitochondria and chloroplasts of eukaryotes and the cytoplasmic membrane of many respiratory and photosynthetic bacteria. BC1 serves two functions—to transfer electrons from ubiquinol to the soluble electron carrier cytochrome *c*, and to generate the proton gradient used to drive ATP synthesis. Given its essential role, BC1 has been the prime target of many antimalarial and antifungal drugs as well as herbicides which are currently widely used [1-4].

Depending on the species, there is variation in the number of polypeptides in the BC1 complex in eukaryotes. However, nearly all BC1 complexes contain three redox proteins: a cytochrome *b* (B) which contains two non-covalently bound *b* hemes (b_L and b_H), a Rieske iron-sulfur protein that contains a [2Fe–2S] cluster and a cytochrome c_1 (C1), which contains one covalently bound heme. Bacterial species have the simplest form of BC1, which consists of a dimer of the three core proteins, and have been used as model systems to study electron transport within BC1 and between BC1 and its electron acceptor (i.e. soluble cytochrome c_2 (C2), membrane-anchored C2 (Cy) or high-potential iron-sulfur protein, HiPIP, in photosynthetic bacteria). Electron transport within the BC1 complex is currently best explained by a Q-cycle mechanism [5,6]. Without going into detail, one electron is transferred from quinol to the b-heme and the other electron to the Rieske [2Fe–2S] cluster, and subsequently to the C1 heme. C1 provides the docking site for the soluble interaction partner (C2, HiPIP) at the membrane–aqueous interface and becomes oxidized.

X-ray crystallographic data from eukaryotic and prokaryotic BC1 complexes have shown that the functional core of BC1 is a dimer, where each monomer is built of the three subunits. While the *b* hemes are positioned in the transmembrane region, the Rieske and C1 subunits from each monomer are anchored to the membrane via a single α-helical transmembrane tail at their N- and C-terminus respectively. The globular domain of each subunit is hydrophilic and resides at the membrane–periplasmic interface [7-12]. Crystallographic studies with and without several bound inhibitors have revealed that

Abbreviations: BC1, ubiquinol cytochrome *c* reductase or Rieske iron–sulfur protein/Cytochrome *b*/Cytochrome c_1 complex; C2, cytochrome c_2; Δfbc, mutant containing a deletion of the whole BC1 operon; RCVB, a minimal growth medium containing mineral salts, essential vitamins, and malate as a carbon source; MOPS, 3-(N-morpholino)-propanesulfonic acid

* Corresponding author at: University of Arizona, Dept. of Chemistry and Biochemistry, 1041 E. Lowell St., Tucson, AZ 85721, USA. Tel.: +1 520 621 5256; fax: +1 520 621 6603.
E-mail address: jkyndt@email.arizona.edu (J.A. Kyndt).
[1] Deceased.

0005-2728/$ – see front matter © 2012 Elsevier B.V. All rights reserved.
doi:10.1016/j.bbabio.2012.01.013

a long-range movement of the head domain of the Rieske subunit is crucial for electron transfer from quinol to the C1 subunit [7,9,13-15]. Since there is no direct interaction between C2 and the Rieske subunit, C1 forms a pivotal connection between the BC1 complex and its soluble electron transfer partners.

Both C2 and C1 belong to the class I *c*-type cytochromes based on their electrochemical and structural properties. *Rhodobacter capsulatus* soluble C2 has been studied intensively by mutagenesis and three dimensional structure analysis. During ligand binding studies, a region of 14 amino acids (positions 89–102), containing the sixth heme ligand (M95), was identified as a 'hinge region' that undergoes rapid large scale motion in ferri-C2, which includes the transient breaking of the Fe-methionyl sulfur bond [16]. The flexibility of the hinge is likely due to its location within a loop between helices.

R. capsulatus and *Rhodobacter sphaeroides* C1 have an analogous loop between helices, residues ~136 to 201, containing the sixth heme ligand M183. The presence of a disulfide bridge within the loop stabilizes it [19] and may reduce the size of the flexible region as shown in the sequence alignment of Fig. 1. It should be noted that such a structure-based alignment of C1 has never been published, thus there are 9 insertions and deletions, three of which are quite large, 10, 17, and 18 residues. Recent imidazole binding studies on C1 within *R. sphaeroides* BC1 suggests the existence of a hinge similar to the C2 hinge, although the exact confines of the flexible region have not been fully defined [17,18]. Structural alignment of *R. capsulatus* C2 and C1 shows that the loop in C1 (orange and cyan sections in Fig. 2), is much larger than in C2. Mutation of both Cys residues to Ala, and the resulting loss of the disulfide bridge, lowers the C1 redox potential (by >300 mV) and results in the loss of photosynthetic growth [19].

Interestingly, the *R. capsulatus* loop contains three consecutive tyrosine residues (Y152–Y154) that are positioned near the interaction site for the C1 reaction partners (Rieske and C2), although they are not highly conserved in eukaryotic C1s. The presence of the 18-residue insertion in the bacterial loop suggests that the dynamics in this region may not be the same for the two groups of C1 and that residues conserved in one group may not be retained in the other. Thus, it may not be possible to generalize conclusions of a single study to the family as a whole. We have postulated, based on structural modeling, that two of these residues, Y152 and Y153 could form a tyrosine bridge that is involved in propagating a conformational change from Rieske, through C1 to C2 [20]. In the model, C1 Y152 is positioned adjacent to the Rieske [2Fe2S] cluster when the latter is in the C1 interacting position, while Y153 is pointing towards the C2 heme. It is therefore plausible that the change in Rieske conformation (from interacting with B to interacting with C1) can exert an effect on the C2 binding via a push–pull mechanism through the C1 tyrosine bridge. In addition, a potential H-bond was identified in the modeled structures between C1 Y153 and C2 T15, which strengthens the hypothesis that this residue could be involved in complex formation during reduction [20]. Y154 is not oriented towards C2 or the Rieske protein, however, it is conserved in all structures, from both prokaryotic and eukaryotic origin, suggesting an important structural or functional role.

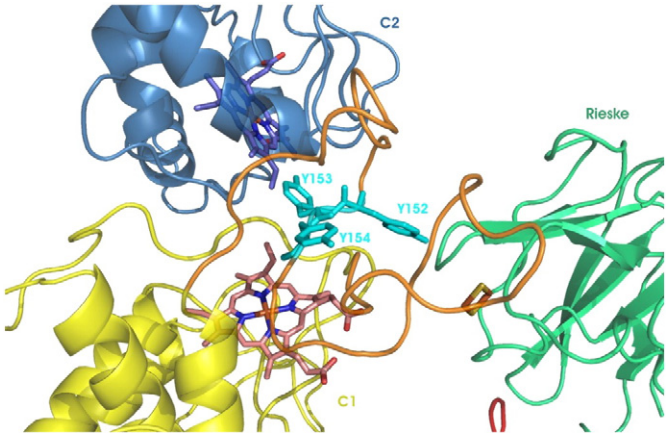

Fig. 2. Structural view of the C2–C1–Rieske interface of *R. capsulatus* BC1, showing the position of the tyrosines (cyan) in the Y-triad. C2 is blue; C1 is yellow, orange and cyan; Rieske protein is green. The extension on C1 as compared to C2 structure is shown in orange and cyan. C1 heme is pink, C2 heme is blue and [2Fe2S] is yellow and orange sticks.

```
                                                HEME
1)    GELELHPPAFPWSHGGPLSALDHSSVRRGFQVYKQVCSACHSMDYVAFRNLIG---VTHTEAEAKALAE
2)    SDLELHPPSYPWSHRGLLSSLDHTSIRRGFQVYKQVCSSCHSMDYVAYRHLVG---VCYTEDEAKALAE
3) MTAAEHGLHAPAYAWSHNGPFETFDHASIRRGYQVYREVCAACHSLDRVAWRTLVG---VSHTNEEVRNMAE
4)       NSNVPDHAFSFEGIFGKYDQAQLRRGFQVYNEVCSACHGMKFVPIRTLADDGGPQLDPTFVREYAA
5)     AGGGHVEDVPFSFEGPFGTFDQHQLQRGLQVYTEVCAACHGMKFVPIRSLSEPGGPELPEDQVRAYAT

1) EVEVQDGPDENGELFMRPGKISDYFPKPYPNPEAARAANNGALPPDLSYIVNARHGG----------------
2) EVEVQDGPNEDGEMFMRPGKLSDYFPKPYPNPEAARAANNGALPPDLSYIVRARHGG----------------
3) EFEYDDEPDEQGNPKKRPGKLSDYIPGPYPNEQAARAANQGALPPDLSLIVKARHGG----------------
4) GLDTI---IDKDSGEERDRKETDMFPTRVG----------DGMGPDLSVMAKARAGFSGPAGSGMNQLFKGM
5) QF-TV---TDEETGEDREGKPTDHFPHSAL----------ENA-PDLSLMAKARAGFHGPMGTGISQLFNGI

                      144        154          167             183
1) --EDYVFSLLTGYCD-PPAGVV--VREGLHYNPYFP------------------GQAIGMAPPIYNEILEYD
2) --EDYVFSLLTGYCD-PPAGVV--VREGLHYNPYFP------------------GQAIGMAPPIYNEVLEFD
3) --CDYIFSLLTGYPDEPPAGVA--LPPGSNYNPYFP------------------GGSIAMARVLFDDMVEYE
4) GGPEYIYNYVIGFEE-NPECAP-EGIDGYYYNKTFQIGGVPDTCKDAAGVKITHGSWARMPPPLVDDQVTYE
5) GGPEYIYSVLTGFPEEPPKCAEGHEPDGFYYNRAFQNGSVPDTCKDANGVKTTAGSWIAMPPPLMDDLVEYA

     200
1) DGTPATMSQIAKDVCTFLRWAAEPEHDQRKRMGLKMLLISALLTSLLYYMKRHKWSVLKSRKMAYRPPK
2) DGTPATMSQVAKDVCTFLRWAAEPEHDHRKRMGLKMLLMMGLLLPLVYAMKRHKWSVLKSRKLAYRPPK
3) DGTPATTSQMAKDVTTFLNWCAEPEHDERKRLGLKTVIILSSLYLLSIWVKKFKWAGIKTRKFVFNPPKPRK
4) DGTPATVDQMAQDVSAFLMWAAEPKLVARKQMGLVAMVMLGLLSVMLYLTNKRLWAPYKGHKA
5) DGHDASVHAMAEDVSAFLMWAAEPKLMARKQAGFTAVMFLTVLSVLLYLTNKRLWAGVKGKKKTNV
```

Fig. 1. Alignment of the C1s for which there are 3-dimensional structures: 1. Chicken, 2. Bovine, 3. Yeast, 4. *R. capsulatus*, 5. *R. sphaeroides*. Numbering is for *R. capsulatus*. Note that the bacterial C1s have a large 18-residue insertion in the region of interest, loop 136–201, that contains the sixth heme ligand Met 183 and the tyrosine triad, 152–154. The disulfide bridge, C144–C167 which helps to stabilize the loop, is conserved in *R. sphaeroides*, but not in the eukaryotic C1s. Helices are underlined. The sixth heme ligand is colored blue and the mutated residues are green.

To test our hypothesis that the C1 tyrosine triad plays a role in overall enzymatic activity from the bacterial Rieske iron–sulfur protein to C2, we have prepared and characterized mutants at C1 positions Y152, Y153 and Y154.

2. Materials and methods

2.1. Growth and cell harvest

R. sphaeroides Δfbc is a strain that has a deleted *fbc* operon (containing the Rieske iron–sulfur protein, cyt b, and cyt c_1) and was generously provided by Prof. A. Crofts. All *R. sphaeroides* Δfbc cultures with *R. capsulatus* complemented BC1 complex were grown on RCVB media with kanamycin and tetracycline antibiotics (to final concentrations of 25 μg/ml and 1.25 μg/ml respectively). All mutant and wild-type *R. capsulatus* BC1 containing plasmids were transformed into the *R. sphaeroides* Δfbc strain by conjugation. Transformed *R. sphaeroides* Δfbc was grown aerobically in the dark (~48 h) and a fresh inoculum was switched to photosynthetic growth under anaerobic conditions (2–3 days, until OD_{550} ~ 1.0). Cells were harvested by centrifugation at 5000 × g for 30 min, and washed once with 50 mM MOPS (pH 7.0), 100 mM KCl and 25% glycerol. Resuspended cells (~1/100 of the initial culture volume) were stored at −80 °C.

2.2. Cloning

A DNA fragment (3950 bp) containing all three genes of the bc_1 operon (Rieske iron–sulfur protein, cyt *b* and cyt c_1), was cloned from *R. capsulatus* genomic DNA using PCR. A second round of PCR was performed to incorporate HindIII and KpnI restriction sites. In addition, the KpnI primer contained a Factor Xa cleavage site and a His-tag sequence, which during PCR is incorporated at the C-terminal end of C1. This PCR resulted in a 3456 bp fragment that contains a 657 bp 5′ and a 44 bp 3′ extension (factor Xa and His-tag) in addition to the three genes of the operon, and has the original *c*1 stop codon omitted. Primers for the second round were: ACCCAAGCTTGAAGATCCTGCTTCTGACCGC (HindIIIRcapsF) and GGGGTACCTTAGTGATGGTGATGGTGGTGCCCGCG CCCCTCAATGGCCTTGTGGCCCTTG (KpnIHisfXaRcapsR). Sequences complementary to the genomic DNA are underlined. Easy-A polymerase was used in both reactions and DNA fragments were purified from gels using the QIAEXII gel purification kit (Qiagen). The resulting HindIII–KpnI fragment was cloned into the pCR-XL-TOPO vector (Invitrogen) after purification, resulting in TOPO (WTbc1His). DNA sequencing showed the presence of all three genes, including the His-tag and promoter region. To reclone the bc_1 operon into pRK415, the TOPO construct was first digested with HindIII and KpnI overnight, after which NcoI was added to digest the remaining TOPO fragment. Without the additional NcoI digest, the TOPO and His-bc_1 fragment are very similar in size and difficult to separate on agarose gels. Digested and purified bc_1-His fragment was then ligated into predigested pRK415. The resulting pRK415(bc1His) was transformed into the *R. sphaeroides* Δfbc strain by conjugation with *Escherichia coli* S17-1 as described [21].

2.3. Mutagenesis

The Quick change site-directed mutagenesis kit (Stratagene) was utilized with changes to the manufacturers' protocol as described [22]. Mutagenesis was performed on TOPO (WTbc1His), with 26–28mer primers to create the desired mutation. After sequencing to confirm the mutation, the complete bc_1 operon was recloned into pRK415 as described above.

2.4. Protein purification

Purification was as described in [23] with the following modifications. Chromatophores were resuspended in buffer A (50 mM MOPS-NaOH, pH 7.0, 100 mM KCl, 20% glycerol), to 2–4 mg protein/ml based on a standard BCA assay (Pierce). MOPS was from Research Products International, Mt. Prospect, Illinois. Chromatophores (10–20 ml per prep) were diluted with 0.3 volumes of Buffer B (50 mM MOPS-NaOH, pH 7.8, 100 mM NaCl, 1 mM $MgSO_4$, and 20% glycerol) to which 1 mg dodecyl maltoside (DM)/mg protein was added from a 10% (w/v) DM solution (Anagrade, D310, >99% pure, Anatrace, Maumee, Ohio). This was incubated with gentle shaking at 4 °C for ~90 min. The solubilized proteins were loaded onto a Ni-NTA resin column (Qiagen) and the flow-through was passed over the column a second time to increase binding efficiency. All purifications were performed at 4 °C and in the presence of protease inhibitors (Calbiochem Protease inhibitor cocktail set V, EDTA-free). The washing and elution of the column were described in [23], with the difference that an additional wash step with buffer C (50 mM MOPS-NaOH, pH 7.8, 100 mM NaCl, 1 mM $MgSO_4$, 0.01% DM) supplemented with 10 mM His was performed to remove additional background absorbance. The BC1 eluted in buffer C supplemented with 200 mM His and 15 μg/ml phosphatidyl choline (PC; Avanti Polar-Lipids Inc.). Purity was checked by SDS-polyacrylamide gel electrophoresis. The BC1 concentration of purified protein was determined based on both the oxidized and reduced Soret peak absorbances ($\varepsilon_{ox} = 375\ mM^{-1}\ cm^{-1}$; $\varepsilon_{red} = 450\ mM^{-1}\ cm^{-1}$) and the average was used for the enzymatic assay. Pyridine hemochrome assays were performed as described [24].

2.5. Enzymatic assay

All solutions were rendered anaerobic by bubbling argon gas through them for at least 30 min. Decylubiquinol (>97% purity, Sigma-Aldrich) was prepared by reducing a 50 μl solution of 25 mM decylubiquinone (in 1:1 ethylene glycol:ethanol) with ~1 mg of sodium borohydride on ice in a stoppered vial. The residual borohydride was neutralized with 2 μl 0.1 M HCl. The decylubiquinol was diluted in an anaerobic buffer (50 mM Tris–HCl, 100 mM NaCl, pH 8.0) to 50 μM, and BC1 was added immediately to a final concentration of 5 nM. An anaerobic solution of 100 μM horse cytochrome *c* was prepared using the same pH 8.0 buffer. The BC1 solution was mixed with oxidized cytochrome *c* (100 μM) using an RX1000 Rapid Kinetics Spectrometer Accessory, and the absorbance was recorded using a Cary 300 spectrophotometer (detection wavelength = 549.5 nm) for 1 min, to determine the reduction of cytochrome *c* by BC1. All assays were done in triplicate at two BC1 concentrations (10 and 15 nM BC1). The initial slope (C reduction) was used to determine initial rates. These rates were divided by the BC1 concentration to obtain the enzymatic activities shown in Table 1.

2.6. Spectroelectrochemistry

Methods for spectroelectrochemical measurements utilized the same instrumentation and the same type of reference electrode (Ag/AgCl, $E_m = -205$ mV vs. SHE) as described [25], and employed the same spectroelectrochemical cell and electrochemical mediators as used previously [26]. Protein solutions (~0.05 mM) for electrochemical studies were prepared as before [27] in 100 mM potassium phosphate buffer at pH 7.5 containing 15 electrochemical mediators and in addition contained ~20% glycerol. As described in detail previously [27] the ratio of oxidized to reduced forms of each redox species is directly related to the absorbances of the optical spectra via Beer's law and so the change in absorbance (in this case the absorbance at 4 nm intervals between 412 and 440 nm) with respect to applied potential can be fit to the Nernst equation (Eq. (1)) using the nonlinear-least-

Table 1
Overview of growth, spectral and catalytic properties of wild-type and mutants of *R. capsulatus* BC1. PS = photosynthetic; catalytic activity is the average of three measurements; + good growth, − no visible growth; n.d. = not determined. Specific activity is a mean value of three experiments and is in nmol cyt *c* reduced per second per nmol BC1. The redox potential of WT was reported by Osyczka et al. [19] and Iwaki et al. [38].

Bc1 variant	PS growth	Soret maximum (nm)	E_m (mV)	Specific activity
Wild type	+	416	+320	19 ± 3.1
Y152Q	+	416	n.d.	17 ± 1.2
Y153F	+	416	+300 ± 20	17 ± 3.0
Y153A	+	413	+205 ± 4	9.9 ± 1.2
Y153Q	+	414	+203 ± 4	1.9 ± 1.0
Y154A	−	410	n.d.	n.d.
Y154A, A181T, A200V	+	414	+238 ± 4	4.0 ± 0.3

squares fitting algorithm in the software Origin©.

$$E_{app} = E_m + 2.303(RT/nF)\log_{10}([Ox]/[Red]) \quad (1)$$

where E_{app} is the applied potential, E_m is the midpoint potential determined from these data, and [Ox] and [Red] are the concentrations in the Fe(III) and Fe(II) states, respectively. Thus, for BC1 with three hemes contributing to the observed absorbances in the optical spectrum, for any applied potential E_{app} the observed change in absorbance due to reduction $\Delta_r A$ at any one wavelength can be written as;

$$\Delta_r A = \frac{\Delta_r A^c}{\left(1 + e^{\frac{E_{app} - E_m^c}{RT/nF}}\right)} + \frac{\Delta_r A^{b_H}}{\left(1 + e^{\frac{E_{app} - E_m^{bH}}{RT/nF}}\right)} + \frac{\Delta_r A^{b_L}}{\left(1 + e^{\frac{E_{app} - E_m^{bL}}{RT/nF}}\right)} \quad (2)$$

where $\Delta_r A^c$ is the total change in absorbance due to heme *c* reduction (extinction coefficient change upon reduction times the total heme *c* concentration times the path-length, $\Delta_r \varepsilon^c$[heme *c*]*l*), and $\Delta_r A^{bH}$ is the total change in absorbance due to heme b_H reduction, and $\Delta_r A^{bL}$ is the total change in absorbance due to heme b_L reduction. The midpoint potentials E_m^c, E_m^{bH}, and E_m^{bL} are for hemes *c*, b_H, and b_L, respectively, and $n = 1$ for a 1 electron heme reduction.

2.7. Structural modeling

A structural model of Y153Q was created by SWISS-model (http://swissmodel. expasy.org//SWISS-MODEL.html). A single template file was used (PDB ID: 1ZRT), which is the structure file for *R. capsulatus* BC1 with stigmatellin bound. The model was generated with ProModII and energy minimization of the model was performed with Gromos96. In silico single point mutations in the *R. capsulatus* BC1 structure (1ZRT) were created in Pymol 0.99 and the builder module was used to predict potential steric clashes.

3. Results

3.1. Mutant growth and spectral analysis

As shown previously, modeling using known structures suggested that three C1 tyrosines are at the C1/C2 interface (Y152, Y153 and Y154) (Fig. 2) [20]. Glutamine mutants of Y152 and Y153 were created to determine the effect of removing the aromatic residue, while maintaining H-bonding capability. Alanine mutations at Y153 and Y154 were chosen to study the deletion of both the aromatic and potential H-bonding, while a phenylalanine mutation at Y153 was designed to test the presence of an aromatic residue without the H-bonding capacity. No visible difference was observed in growth rate between wild-type and the BC1 mutants except for the Y154A mutant cultures (see Table 1). *R. sphaeroides* Δ*fbc* supplemented with the pRK415(*fbc* Y154A) plasmid showed no growth under photosynthetic conditions. In one instance however, abnormal growth with a lag phase lasting ~2 months was observed. The plasmid was extracted from this culture and sequenced, revealing two unintended mutations. One was A181T and the other was A200V. Mass spectrometric analysis confirmed the existence of all three mutations in the one protein.

After purification, all of the BC1 mutants showed similar patterns on Coomassie blue stained SDS-PAGE gels under denaturing conditions. In-gel tryptic digests followed by mass spectrometric analysis showed that the three bands on the gel corresponded to cytochrome *b*, cytochrome c_1 and Rieske protein. As observed previously, the SDS-PAGE gel pattern for cytochrome *b* could only be observed if the sample was not boiled before loading (Fig. 3A). The pyridine hemochromogen assay [24] yielded the same *b* to *c* heme ratios for the mutants and wild-type, consistent with both cytochrome *c* and *b* being fully reconstituted in all mutants although the peaks were not resolved nor quantified.

Using ascorbate reduced minus ferricyanide oxidized difference spectra, we found the Y152Q and Y153F BC1 mutants having similar levels of high potential C1 alpha peaks as wild-type (compare Fig. 3B, C and F) as well as Soret wavelength maxima in dithionite minus air oxidized spectra (Table 1). In contrast, the Y153A and Y153Q mutants had blue-shifted Soret wavelength maxima (to 413 and 414 respectively, versus 416 nm for WT; see Table 1) and showed significantly less C1 reduction by ascorbate (by ca 0.5 and 0.75 respectively, compare Fig. 3B, D and E), in spite of having wild-type amounts of *c*-type heme based on pyridine hemochrome spectra. Wild-type and all four mutants had similar dithionite reduced minus ferricyanide difference spectra in the *b*-type cytochrome alpha peak region (~560 nm), but Y153A and Q mutants had significantly smaller alpha peaks in the 550 nm region characteristic of low-spin *c*-type cytochrome. By inference, the reduced amount of alpha peak absorbance with ascorbate and no additional amount with dithionite suggests that the remainder of the heme is high spin. Dithionite minus ascorbate difference spectra for wild type BC1 and Y153F are consistent with little or no *c*-type heme that is not ascorbate reducible, as expected (supplemental information Fig. S1). Difference spectra for mutants Y153Q and Y153A showed a similar pattern and indicate that only a minor fraction of the C1 reduced further with dithionite than what had already been reduced with ascorbate (Fig. S1). To summarize in terms of spectral properties, Y152Q and Y153F appear to be essentially identical to wild-type. However, the *c*-heme of Y153A and Q is only partially reducible, by either ascorbate or dithionite. This suggests a mixture of conformations, most likely resulting from the presence of both low- and high-spin c-type hemes corresponding to protein with and without an attached sixth ligand.

Mutation of the most conserved residue in the Y-triad, Y154, to A resulted in very low production of BC1 and only small amounts could be isolated from aerobically grown cultures which rapidly degraded during purification. The low yield and instability prevented complete purification of this mutant, but spectra indicated a blue-shifted Soret peak of about 410 nm due to misfolding (Table 1). On the other hand, the spontaneous second-site revertant mutant (Y154A, A181T, A200V) resulted in sufficient purified protein to obtain useful data. When compared to wild-type spectra, the triple

Fig. 3. A. SDS-page gel for wild-type *R. capsulatus* BC1, purified using a TALON (Ni-NTA resin) affinity column (M = marker). B–G. Reduced minus oxidized difference spectra of *R. capsulatus* BC1. Spectra were taken in 50 mM MOPS (pH 7.8, 20% glycerol, 100 mM NaCl, 1 mM MgCl2, 0.01% DM and 15 μg/ml PC). Figures B–G are taken in the α–β peak region. Samples were oxidized with ferricyanide and reduced with ascorbate and subsequently with dithionite. Black traces show dithionite-reduced minus ferricyanide-oxidized spectra, red lines show ascorbate-reduced minus ferricyanide-oxidized spectra. Panel B: WT; panel C: Y152Q; panel D: Y153A; panel E: Y153Q; panel F: Y153F; panel G: (Y154A, A181T, A200V) mutant.

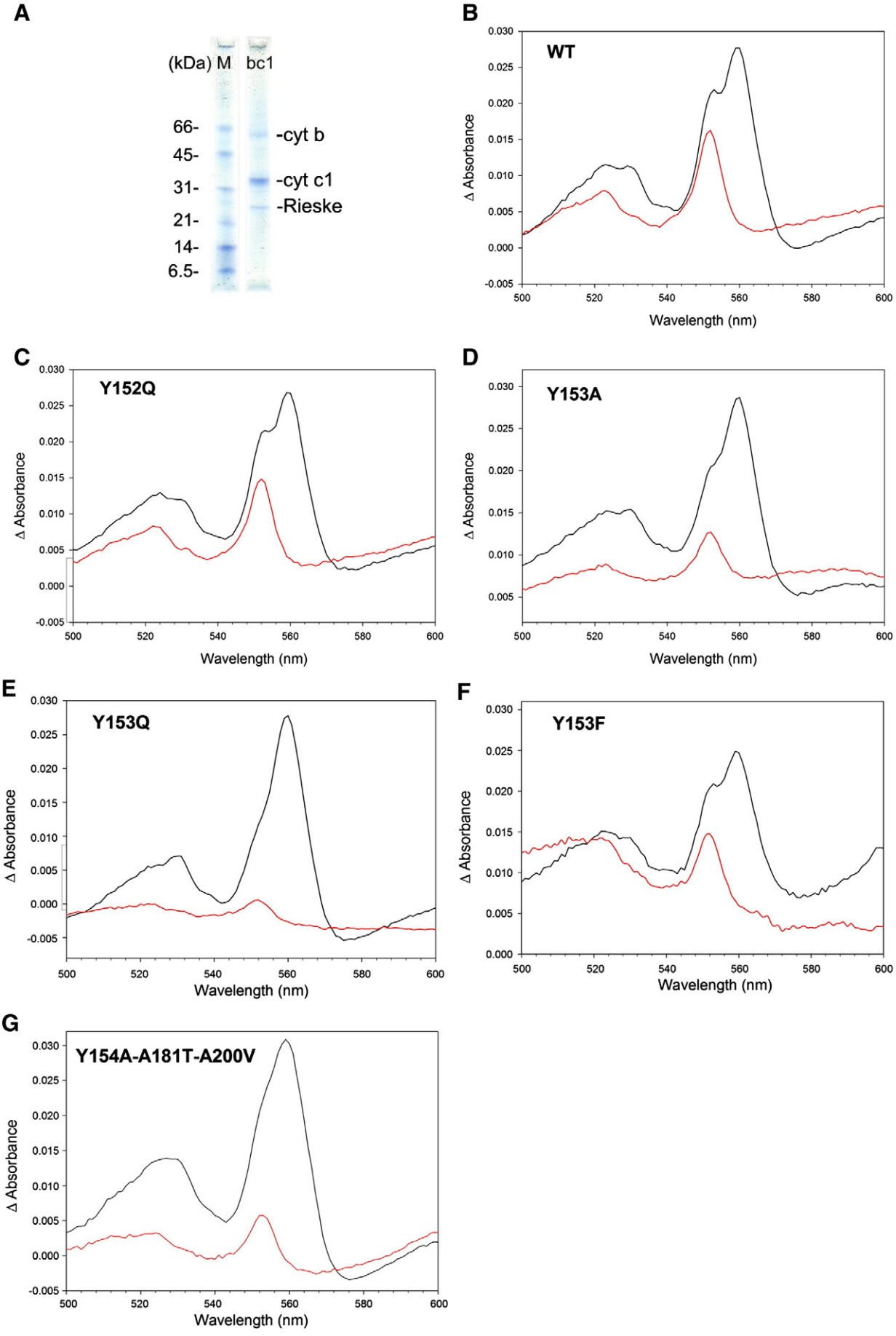
A
(kDa) M bc1
66-
45-
31-
21-
14-
6.5-
-cyt b
-cyt c1
-Rieske
B
WT
C
Y152Q
D
Y153A
E
Y153Q
F
Y153F
G
Y154A-A181T-A200V
Δ Absorbance
Wavelength (nm)

mutant showed about 2- to 3-fold decrease in ascorbate reduction (Fig. 3G). The Soret peak in this mutant was less blue-shifted than in the Y154A single mutant, but similar to the Y153A and Q mutants. In addition, the dithionite minus ascorbate difference spectrum is also similar to wild-type (Fig. S1).

3.2. Midpoint potentials

To further characterize the mutants, we performed spectroelectrochemical titrations. Upon titration of BC1 from +255 to +115 mV vs. SHE, we mainly observed *c* heme reduction with the beginning of *b* heme reduction, and over the range of +155 to −15 mV vs. SHE we observed the start of *b* heme reduction. Titration data are given in supplemental figures (S2A–D). From these titrations we were able to determine the heme midpoint potentials as described in the methods section (Table 1). The potential titration range chosen was optimal for accurate determination of the *c* heme midpoint potentials and typically covered sufficient reduction of the *b* hemes to allow deconvolution of the *c* heme absorbances from the *b* hemes using Eq. (2). Typical midpoint potentials for cytochrome *b* were about −77 mV for heme b_L and +44 mV (vs. SHE) for heme b_H, which agree reasonably well with previously reported values for WT BC1 [28]. For the *c* heme, the potential of Y153F was similar to the reported WT value and should be taken as the point of reference for the other mutants. The derived midpoint potential for Y153Q was +203 mV (vs. SHE). This value is about 97 mV lower than Y153F and 117 mV lower than the reported WT value of +320 mV [19]. Y153A had the same *c* heme midpoint potential (+205 mV vs. SHE) as Y153Q, and the triple mutant had a slightly higher midpoint potential of +238 mV (about 62 mV lower than Y153F).

3.3. Catalytic analysis

The catalysis of the oxidation of decylubiquinol and reduction of horse cytochrome *c* by BC1 was used to determine enzymatic activity [29]. Horse C and *R. capsulatus* C2 have similar tertiary structures and the kinetic values for reduction by *R. capsulatus* BC1 are nearly identical [29]. Since horse C is more readily available, it was used in *Rhodobacter* BC1 activity assays. The results are provided in Table 1. The wild-type activity was in the range of that published for *R. capsulatus* and *R. sphaeroides* His-tagged purified BC1 [30]. Moreover, the Y152Q and Y153F activities were identical to wild-type BC1 within experimental error, which implies that these mutations do not change the structure or electrochemistry of C1 to a degree that affects the function of the BC1. This also implies that the His tag has a minimal effect on activity although this was not explicitly tested. However, the Y153Q mutation significantly lowered the enzymatic activity of BC1 by ten-fold and the Y153A mutation lowered it two-fold. We were unable to obtain sufficient material for the Y154A mutant to measure C2 reduction, however, the (Y154A, A181T, A200V) triple mutant showed about a five-fold reduction in specific activity (Table 1).

4. Discussion

Modeling of the *R. capsulatus* BC1 structure with the Rieske protein complexed with C1 or with B and subsequent docking with C2, led us to propose that a triad of tyrosine residues in C1 (Y152–Y154) could play a role in mediating binding and electron flow from the Rieske protein to the C2 [20]. Y152 points directly towards the Rieske protein and is in close proximity to the iron–sulfur center in the C1 bound position (Fig. 2). Y153 is oriented towards C2, it is solvent exposed and, at least in the docking experiments, is within H-bonding distance of the C2 T15 hydroxyl. However, Y153 is not conserved in yeast BC1, and the structure of the yeast BC1/C complex with bound yeast C shows that the main interactions stabilizing the complex are non-polar in nature and only two direct polar interactions are present in the binding domain [8,12]. Y154 is not oriented towards C2 or the Rieske protein, however, it is the most conserved of the three tyrosines amongst different species and may therefore play an essential structural role.

As reported here, mutation of residue Y152 to Q has little or no effect on the electrochemical properties or on the enzymatic activity of BC1. This is consistent with the finding that a C1 Y152R mutation allowed for normal photosynthetic growth of *R. capsulatus* [19]. The fact that, in the modeled *R. capsulatus* structure, where the Rieske protein is bound to C1, Y152 is positioned close to both the C1 heme and the Rieske 2Fe2S cluster, raised the possibility that the aromatic ring could be indirectly involved in electron transfer between the two cofactors [20]. As far we can tell, there is no evidence in our assays that this electron transfer has been significantly impaired by the loss of the aromatic residue at position Y152.

It was proposed previously, based on the bovine BC1 crystal structure, that electron transfer from the Rieske 2Fe2S cluster occurs through the bovine Rieske residue His 161 [31]. This residue forms a hydrogen bond with one of the propionates of heme C1 when Rieske is in the C position. The corresponding His residue (156) is conserved in Rhodobacter BC1 and we therefore speculate it might have the same role.

Mutation of C1 Y153 did result in a BC1 with very distinct properties compared to wild-type. Mutation of Y153 to Q resulted in a spectrally different BC1, where the intensities of the C1 α and β peaks were significantly lower than in wild-type C1 upon reduction. To a lesser degree, this was also observed in the Y153A mutant. Measuring the redox midpoint potential (E_m) for Y153Q showed that the E_m was lowered to 203 mV for the C1 heme, while the cyt *b* heme values were similar to WT. Although this is a significant difference in redox potential for C1, it is not sufficient to explain the lower magnitude of α and β peaks upon reduction, since it is still considerably more positive than the ascorbate redox potential of +60 mV (at pH 7). The results rather suggest that the remaining heme is high spin. The fact that we observe a small blue-shift in the Soret region with Y153A and Y153Q, is consistent with the possibility that a certain amount of high-spin C1 is present in these mutants, besides the lower potential C1 population.

Very similar results were obtained with mutations made at position F138 to non-aromatic amino acids [32]. Additional experiments with those mutants showed that besides significantly lower E_m values and lower magnitude of α and β peaks upon reduction, these mutants also displayed altered EPR spectra. Therefore, in both the Y153 and F138 mutants, redox and spin-state heterogeneity are likely to be the cause of the observed spectral differences. F138 is structurally just as close to the C1 hinge region as Y153, although it is oriented inwards as opposed to Y153 which points out towards C2. Nevertheless, the close proximity of both residues to the hinge region, which contains the sixth heme ligand, lead us to believe that both residues are involved in structural stabilization of the hinge region to maintain optimal spectral and catalytic properties.

When examining one of the structures in the C1 hinge region, it can be seen that Y153 is closely packed against the proline residue (P184) that is next to the sixth heme ligand (M183) (Fig. 4). The closest carbon atoms of the Y153 and P184 rings are only 3.6 Å apart and the planes of the rings are almost parallel to each other. This suggests a stabilizing packing between the two side chains. Such packing of aromatic residues against the proline ring has been observed and studied before in other proteins and is often found in type VI reverse turns when the aromatic residue and the proline residue are positioned sequentially [33,34]. Thermodynamic calculations and computer simulations of Tyr-Pro interactions in isolated peptides have shown that the interaction is relatively strong and provide high stability to the folded peptide [35,36]. We therefore believe that the Y153-P184 ring packing in C1 is important to provide stability to

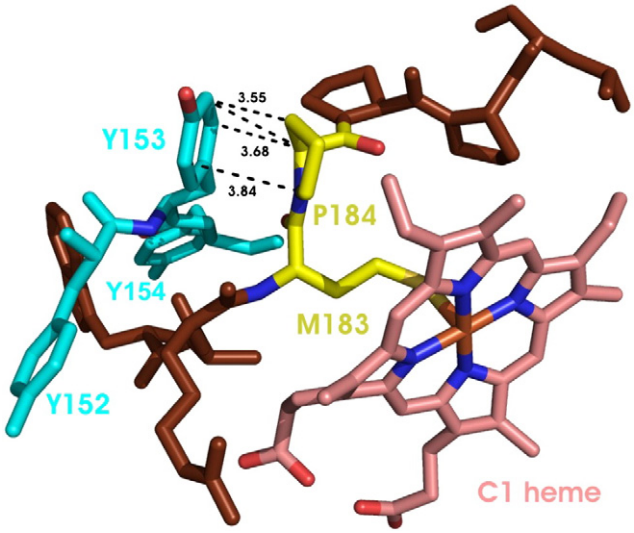

Fig. 4. Detailed structural view of the C1 heme and hinge region. Hinge region is shown in brown, Y-triad in cyan and C1 heme in pink. Y153 is packed closely to P184, which is adjacent to the sixth heme ligand M183. Distances between carbon atoms (in Å) are labeled in black.

the C1 hinge region and keeps M183 positioned optimally for heme interaction.

The Y153–P184 interaction is consistent with the fact that the spectra and E_m values we obtained with the Y153F mutant are similar to wild-type BC1. In this mutant, the aromatic-Pro packing is still expected to occur, and no perturbation of the C1 heme region is expected. By packing with P184, Y153 is bent in an almost cis conformation. When a structural model was created in silico for the BC1 complex with the C1 Y153Q mutant, it became clear that a simple, backbone-independent, replacement of Y with Q at that position creates steric clashes between Q153 and residues of the hinge region, which would result in some backbone adjustment. Mutation of Y153 to A does not create the observed steric clashes in our model, however it will create an increased mobility in the hinge region, by removal of the supporting aromatic/proline interaction. This is not expected to be as detrimental as the Q mutation, which is reflected in the slightly less-pronounced spectral changes we observed in the Y153A mutant versus Y153Q.

In addition to the spectral changes, the Y153Q mutation also created a 10-fold less catalytically efficient BC1. The redox heterogeneity of C1 (created by Y153 mutation), in which less reducible C1 is present, could result in lower efficiency of overall C reduction, or the structural interaction with C2 is impaired by removal of Y153, or a combination of both. The following facts, however, argue against an altered C2 interaction as the basis for the lower activity. First, the Y153-T15 hydrogen bond in the docked *R. capsulatus* model could still be achieved by Q (although it might be weakened and the hinge region would have to move significantly). However, the enzymatic activity is only reduced two-fold in Y153A versus ten-fold in Y153Q, while the A mutation is clearly incapable of forming a H-bond with C2 and therefore the activity would be expected to be even lower than in the Y153Q mutant if an impaired C2 interaction were the basis for the lower activity. Secondly, kinetics of C2 reduction with the Y153F mutant are essentially the same as wild-type, which indicates that the aromatic properties of Y153 are more important than potential H-bonding with C2. This is consistent with the conclusion that the aromatic residue is necessary to maintain hinge region stability and normal redox properties. We therefore conclude that the lower activity is due to the redox heterogeneity of the Y153 mutants, which is linked to the structural perturbation of the hinge region. The fact that Y153A has higher activity than Y153Q indicates that there is less structural perturbation in Y153A or that more molecules can obtain the WT conformation at a given time.

Y154 is also part of the Y-triad and although it is not positioned for interaction with any of the C1 interaction partners, it is the most conserved tyrosine residue of the three. It is conserved in BC1 structures from every species examined to date. To investigate whether this residue has a structural function, we mutated it to an alanine residue. Production yields and initial spectral analysis clearly indicate that, upon removal of this residue, the BC1 is significantly destabilized and most likely no longer functional in the cells, given the lack of photosynthetic growth of *Rhodobacter* Δfbc species complemented with this BC1 mutant. This proves the structural necessity for this residue at position 154 in *R. capsulatus* BC1 and, given its conserved nature, also at equivalent positions in BC1 from other species. However, slowly growing cultures were able to compensate for this loss of function by spontaneously introducing two additional mutations (A181T and A200V). When the triple mutant protein was purified and characterized, it displayed significantly lower catalytic activity, reduction by ascorbate, and lower E_m (~62 mV lower than Y153F). Interestingly, these two unintended mutations are on both sides of the region we presumed to be the 'hinge region' of C1 based on homology with the C2 hinge. It is intriguing that one of these mutations (A181T) also spontaneously occurred upon deletion of the Cys144–Cys167 bridge that is part of the extended loop [19]. Upon introduction of this mutation in wild type, a functional BC1 with lowered E_m (~100 mV lower than wild type) was created [37]. The latter behaved very similarly to the triple mutant created in this study. Although the exact function of these spontaneous mutations remains unknown, it is plausible that they restore BC1 activity by stabilizing the hinge region and the position of the sixth ligand. Although activity was not fully restored in the triple mutant, it appears to be sufficient to produce a functional BC1 in growing cells.

Supplementary materials related to this article can be found online at doi:10.1016/j.bbabio.2012.01.013.

Acknowledgement

This work was supported by a grant from the National Institutes of Health (GM21277).

References

[1] M.W. Mather, E. Darrouzet, M. Valkova-Valchanova, J.W. Cooley, M.T. McIntosh, F. Daldal, A.B. Vaidya, Uncovering the molecular mode of action of the antimalarial drug atovaquone using a bacterial system, J. Biol. Chem. 280 (2005) 27458–27465.
[2] C.L. Yeates, J.F. Batchelor, E.C. Capon, N.J. Cheesman, M. Fry, A.T. Hudson, M. Pudney, H. Trimming, J. Woolven, J.M. Bueno, J. Chicarro, E. Fernandez, J.M. Fiandor, D. Gargallo-Viola, F. Gomez de las Heras, E. Herreros, M.L. Leon, Synthesis and structure–activity relationships of 4-pyridones as potential antimalarials, J. Med. Chem. 51 (2008) 2845–2852.
[3] D.W. Barlett, J.M. Clough, J.R. Godwin, A.A. Hall, M. Hamer, B. Parr-Dobrzanski, The strobilurin fungicides, Pest Manag. Sci. 58 (2002) 649–662.
[4] D.B. Jordan, K.T. Kranis, M.A. Picollelli, R.S. Schwartz, J.A. Sternberg, K.M. Sun, Famoxadone and oxazolidinones: potent inhibitors of cytochrome bc_1, Biochem. Soc. Trans. 27 (1999) 577–580.
[5] J. Zhu, T. Egawa, S. Yeh, L. Yu, C. Yu, Simultaneous reduction of iron–sulfur protein and cytochrome bL during ubiquinol oxidation in cytochrome bc1 complex, Proc. Natl. Acad. Sci. U. S. A. 104 (2007) 4864–4869.
[6] C.H. Snyder, E.B. Gutierrez-Cirlos, B.L. Trumpower, Evidence for a concerted mechanism of ubiquinol oxidation by the cytochrome bc_1 complex, J. Biol. Chem. 275 (2000) 13535–13541.
[7] Z. Zhang, L. Huang, V.M. Shulmeister, Y. Chi, K.K. Kim, L. Hung, A.R. Crofts, E.A. Berry, S. Kim, Electron transfer by domain movement in cytochrome bc_1, Nature 392 (1998) 677–684.
[8] C. Lange, C. Hunte, Crystal structure of the yeast cytochrome bc1 complex with its bound substrate cytochrome *c*, Proc. Natl. Acad. Sci. USA 99 (2002) 2800–2805.
[9] E.A. Berry, L.S. Huang, L.K. Saechoa, N.G. Pon, M. Valkova-Valchanova, F. Daldal, X-ray structure of *Rhodobacter capsulatus* cytochrome bc_1: comparison of its mitochondrial and chloroplast counterparts, Photosynth. Res. 81 (2004) 251–275.
[10] L.S. Huang, D. Cobessi, E.Y. Tung, E.A. Berry, Binding of the respiratory chain inhibitor antimycin to the mitochondrial *bc*1 complex: a new crystal structure reveals

an altered intramolecular hydrogen bonding pattern, J. Mol. Biol. 351 (2005) 573–597.
[11] L. Esser, M. Elberry, F. Zhou, C. Yu, L. Yu, D. Xia, Inhibitor-complexed structures of the cytochrome bc1 from the photosynthetic bacterium *Rhodobacter sphaeroides*, J. Biol. Chem. 283 (2008) 2846–2857.
[12] S.R. Solmaz, C. Hunte, Structure of complex III with bound cytochrome *c* in reduced state and definition of a minimal core interface for electron transfer, J. Biol. Chem. 283 (2008) 17542–17549.
[13] D. Xia, C. Hu, H. Kim, J. Xia, A.M. Kachurin, L. Zhang, L. Yu, J. Deisenhofer, Crystal structure of the cytochrome bc_1 complex from bovine heart mitochrondria, Science 277 (1997) 60–66.
[14] A.R. Crofts, M. Guergova-Kuras, L.S. Huang, R. Kuras, Z. Zhang, E.A. Berry, Mechanism of ubiquinol oxidation by the bc_1 complex: role of the iron sulfur protein and its mobility, Biochemistry 38 (1999) 15791–15806.
[15] E. Darrouzet, F. Daldal, Movement of the iron–sulfur subunit beyond the ef loop of cytochrome *b* is required for multiple turnovers of the bc_1 complex but not for single turnover Q_o site catalysis, J. Biol. Chem. 277 (2001) 3471–3476.
[16] C. Dumortier, H. Remaut, J.C. Fitch, T.E. Meyer, J.J. Van Beeumen, M.A. Cusanovich, Protein dynamics in the region of the sixth ligand methionine revealed by studies of imidazole binding to *Rhodobacter capsulatus* cytochrome c_2 hinge mutants, Biochemistry 43 (2004) 7717–7724.
[17] O. Kokhan, V.P. Shinkarev, C.A. Wraight, Binding of imidazole to the heme of cytochrome *c*1 and inhibition of the *bc*1 complex from *Rhodobacter sphaeroides*. I. Equilibrium and modeling studies, J. Biol. Chem. 285 (2010) 22513–22521.
[18] O. Kokhan, V.P. Shinkarev, C.A. Wraight, Binding of imidazole to the heme of cytochrome *c*1 and inhibition of the *bc*1 complex from *Rhodobacter sphaeroides*. II. Kinetics and mechanism of binding, J. Biol. Chem. 285 (2010) 22522–22531.
[19] A. Osyczka, P.L. Dutton, C.C. Moser, E. Darrouzet, F. Daldal, Controlling the functionality of cytochrome c_1 redox potentials in the *Rhodobacter capsulatus* bc_1 complex through disulfide anchoring of a loop and a beta-branched amino acid near the heme-ligating methionine, Biochemistry 40 (2001) 14547–14556.
[20] S. Devanathan, Z. Salamon, G. Tollin, J.C. Fitch, T.E. Meyer, E.A. Berry, M.A. Cusanovich, Plasmon waveguide resonance spectroscopic evidence for differential binding of oxidized and reduced *Rhodobacter capsulatus* cytochrome c_2 to the cytochrome bc_1 complex mediated by the conformation of the Rieske iron–sulfur protein, Biochemistry 46 (2007) 7138–7145.
[21] J. Davis, T.J. Donohue, S. Kaplan, Construction, characterization and complementation of a Puf-mutant of *Rhodobacter sphaeroides*, J. Bacteriol. 170 (1998) 320–329.
[22] J.A. Kyndt, J.K. Hurley, B. Devreese, T.E. Meyer, M.A. Cusanovich, G. Tollin, J.J. Van Beeumen, *Rhodobacter capsulatus* photoactive yellow protein: genetic context, spectral and kinetics characterization, and mutagenesis, Biochemistry 43 (2004) 1809–1820.
[23] M. Guergova-Kuras, R. Salcedo-Hernandez, G. Bechmann, R. Kuras, R.B. Gennis, A.R. Crofts, Expression and one-step purification of a fully active polyhistidine tagged cytochrome bc_1 complex from *Rhodobacter sphaeroides*, Prot. Expr. Purif. 15 (1999) 370–380.
[24] E.A. Berry, B.L. Trumpower, Simultaneous determination of hemes *a, b*, and *c* from pyridine hemochrome spectra, Anal. Biochem. 161 (1987) 1–15.
[25] X.D. Ding, A. Weichsel, J.F. Andersen, T.K. Shokhireva, C. Balfour, A.J. Pierik, B.A. Averill, W.R. Montfort, F.A. Walker, Nitric oxide binding to the ferri- and ferroheme states of nitrophorin 1, a reversible NO-binding heme protein from the saliva of the blood-sucking insect, *Rhodnius prolixus*, J. Am. Chem. Soc. 121 (1999) 128–138.
[26] K. Johnson-Winters, A.R. Nordstrom, S. Emesh, A.V. Astashkin, A. Rajapakshe, R.E. Berry, G. Tollin, J.H. Enemark, Effects of interdomain tether length and flexibility on the kinetics of intramolecular electron transfer in human sulfite oxidase, Biochemistry 49 (2010) 1290–1296.
[27] R.E. Berry, T.K. Shokhireva, I. Filippov, M.N. Shokhirev, H. Zhang, F.A. Walker, Effect of the N-terminus on heme cavity structure, ligand equilibrium, rate constants, and reduction potentials of nitrophorin 2 from *Rhodnius prolixus*, Biochemistry 46 (2007) 6830–6843.
[28] A.R. Crofts, C.A. Wraight, The electrochemical domain of photosynthesis, Biochim. Biophys. Acta 726 (1983) 149–185.
[29] S. Güner, A. Willie, F. Millet, M.S. Caffrey, M.A. Cusanovich, D.E. Robertson, D.B. Knaff, The interaction between cytochrome c_2 and the cytochrome bc_1 complex in the photosynthetic purple bacteria *Rhodobacter capsulatus* and *Rhodopseudomonas viridis*, Biochemistry 32 (1993) 4793–4800.
[30] X. Gong, L. Yu, D. Xia, C.A. Yu, Evidence for electron equilibrium between the two hemes b_L in the dimeric cytochrome bc_1 complex, J. Biol. Chem. 280 (2005) 9251–9257.
[31] S. Iwata, J.W. Lee, K. Okada, J.K. Lee, M. Iwata, B. Rasmussen, T.A. Link, S. Ramaswamy, B.K. Jap, Complete structure of the 11-subunit bovine mitochondrial cytochrome bc1 complex, Science 281 (1998) 64–71.
[32] J. Li, A. Osyczka, R.C. Conover, M.K. Johnson, H. Qin, F. Daldal, D.B. Knaff, Role of acidic and aromatic amino acids in *Rhodobacter capsulatus* cytochrome *c*. A site directed mutagenesis study, Biochemistry 42 (2003) 8818–8830.
[33] J. Yao, J.H. Dyson, P.E. Wright, Three-dimensional structure of a type VI turn in a linear peptide in water solution. Evidence for stacking of aromatic rings as a major stabilizing factor, J. Mol. Biol. 243 (1994) 754–766.
[34] M.W. MacArthur, J.M. Thornton, Influence of proline residues on protein conformation, J. Mol. Biol. 218 (1991) 397–412.
[35] E. Demchuk, D. Bashford, D.A. Case, Dynamics of a type VI reverse turn in a linear peptide in aqueous solution, Fold. Des. 2 (1997) 35–46.
[36] E. Demchuk, D. Bashford, G.P. Gippert, D.A. Case, Thermodynamics of a reverse turn motif. Solvent effects and side-chain packing, J. Mol. Biol. 270 (1997) 305–317.
[37] E. Cieluch, K. Pietryga, M. Sarewicz, A. Osyczka, Visualizing changes in electron distribution in coupled chains of cytochrome *bc*1 by modifying barrier for electron transfer between the FeS cluster and heme *c*1, Biochim. Biophys. Acta 1797 (2010) 296–303.
[38] M. Iwaki, A. Osyczka, C.C. Moser, P.L. Dutton, R.R. Rich, ATR–FTIR spectroscopy studies of iron–sulfur protein and cytochrome c1 in the *Rhodobacter capsulatus* cytochrome bc1 complex, Biochemistry 43 (2004) 9477–9486.